Hindawi Publishing Corporation
Mathematical Problems in Engineering
Volume 2014, Article ID 870936, 15 pages
http://dx.doi.org/10.1155/2014/870936

Research Article

Change Detection in Synthetic Aperture Radar Images Based on Fuzzy Active Contour Models and Genetic Algorithms

Jiao Shi,[1] Jiaji Wu,[1] Anand Paul,[2] Licheng Jiao,[1] and Maoguo Gong[1]

[1] *Key Laboratory of Intelligent Perception and Image Understanding of Ministry of Education, Institute of Intelligent Information Processing, Xidian University, Xi'an, Shaanxi 710071, China*
[2] *School of Computer Science Engineering, Kyungpook National University, Daegu 702-701, Republic of Korea*

Correspondence should be addressed to Jiao Shi; jsjiaoshi@gmail.com

Received 20 December 2013; Accepted 8 March 2014; Published 9 April 2014

Academic Editor: Albert Victoire

Copyright © 2014 Jiao Shi et al. This is an open access article distributed under the Creative Commons Attribution License, which permits unrestricted use, distribution, and reproduction in any medium, provided the original work is properly cited.

This paper presents an unsupervised change detection approach for synthetic aperture radar images based on a fuzzy active contour model and a genetic algorithm. The aim is to partition the difference image which is generated from multitemporal satellite images into changed and unchanged regions. Fuzzy technique is an appropriate approach to analyze the difference image where regions are not always statistically homogeneous. Since interval type-2 fuzzy sets are well-suited for modeling various uncertainties in comparison to traditional fuzzy sets, they are combined with active contour methodology for properly modeling uncertainties in the difference image. The interval type-2 fuzzy active contour model is designed to provide preliminary analysis of the difference image by generating intermediate change detection masks. Each intermediate change detection mask has a cost value. A genetic algorithm is employed to find the final change detection mask with the minimum cost value by evolving the realization of intermediate change detection masks. Experimental results on real synthetic aperture radar images demonstrate that change detection results obtained by the improved fuzzy active contour model exhibits less error than previous approaches.

1. Introduction

Image change detection is a process for identifying change regions in images of the same geographical area which are taken at different times. It has attracted widespread interest due to a large number of applications, such as remote sensing [1–3], medical diagnosis [4], and video surveillance [5, 6]. More in particular, synthetic aperture radar (SAR) is of great use due to its independence of critical atmospheric circumstances, day/night conditions of illumination, and weather conditions. Change detection which is one of the fundamental tasks in the interpretation and understanding of SAR images has been widely used in real applications, such as agricultural survey [7], forest monitoring [8], natural disaster monitoring [9], and urban change analysis [10].

Traditional change detection methods can be divided into two kinds: supervised methods and unsupervised methods. Supervised methods need labeled samples for training the classifier, while unsupervised methods do not need labeled samples. In real applications, it may be impossible to obtain the ground truth, which makes unsupervised methods become more popular than supervised ones. Unsupervised change detection approaches of SAR images are mainly summarized into three steps: (1) image preprocessing, (2) generating the difference image, and (3) analyzing the difference image (DI). Geometric correction and registration are often conducted as part of the first step to get the various images aligned within the same coordinate frame. In the second step, two coregistered images are compared to generate the DI. In the third step, the analysis of the DI can be taken as an image segmentation process for partitioning the DI into changed and unchanged regions.

Change regions are usually detected by applying threshold methods for finding a decision threshold to the histogram of the DI. However, some essential models have to be established in advance before being able to determine the best threshold. The need of prior assumptions in modeling the DI makes threshold methods unsuitable for change detection on different types of SAR images. In order to overcome limitations imposed by estimating statistical models for changed

and unchanged regions, one needs to design an unsupervised and distribution-free change detection method which can be applied to different types of satellite images.

In the literature, various techniques have been proposed for image segmentation, such as histogram-based methods, clustering methods, and mathematical morphology [11], among which active contour models (ACMs) [12] are well-known technique in image segmentation [13–19]. The core part of ACMs for image segmentation is that a curve is being employed as a contour, while it is being adapted subject to characteristics from the image, and then objects can be extracted by optimizing an energy function. Edge detection has been successfully applied to many fields, such as feature extraction, image registration, object detection, and motion tracking [9–16]. There is no need for ACMs to establish statistical models, so it seems to be rather convenient and feasible to apply ACMs to different types of satellite images.

The performance of classical ACMs, which use energy functions on the basis of edge information, is inadequate since only objects with edges expressed in terms of gradients can be detected [19, 20]. For comparison, many enhanced models have been proposed on designing complex region-based energy functions, which are less sensitive to noise and can detect objects with weak boundaries [21–23]. Although they enjoy excellent performance, defects within these models are still not fully eliminated. A detrimental condition for many ACMs is that they are defined as the partition of an image into nonoverlapped and consistent regions which are homogeneous with respect to some image characteristics such as gray value or texture. However, it may be impossible to obtain real SAR images with nonoverlapped and consistent regions. Issues such as limited spatial resolution, noise, and overlapping intensities may reduce the effectiveness of traditional ACMs on SAR images.

Generally, DIs are not easily separated into changed and unchanged regions by sharp boundaries. Fuzzy logic, a classical soft computing technique, can process information in a flexible manner that well meets the demand of practical applications [24–32]. Compared with ACMs using hard energy functions, ACMs using fuzzy energy functions have the potential to avoid being trapped into local minima and can better handle objects whose boundaries are not necessarily expressed in terms of gradients [17]. However, traditional fuzzy sets tend to capture vagueness through precise numeric membership degrees which are calculated depending on a single fuzzy coefficient. This poses a contradiction of excessive precision in describing uncertain phenomenon. Membership degrees are more reasonable to be taken as uncertain instead of as certain in traditional fuzzy sets.

Interval type-2 fuzzy sets, as an extension of traditional fuzzy sets, introduce a secondary membership to define the possibilities of the primary membership. It can generate uncertain membership degrees by using two fuzzy coefficients [33]. Interval type-2 fuzzy sets have shown their effectiveness in handling uncertainties in comparison to traditional fuzzy sets. However, the selection of fuzzy coefficients has great impact on final results and requires careful consideration in practical applications. Therefore, the issue on selecting fuzzy coefficients needs careful attention when employing interval type-2 fuzzy set-based algorithms.

Addressing uncertainty through using interval type-2 fuzzy sets has been applied to various fields where we cannot obtain satisfactory performance by traditional fuzzy sets, such as control of mobile robots, inference engine design, transport scheduling, and pattern recognition [34–37]. However, very little effort has been made on combining interval type-2 fuzzy sets with active contour methodology. If we can properly model uncertainties in the DI with the help of interval type-2 fuzzy sets, it is strongly expected to be possible to design an enhanced change detection approach for SAR images. In this paper, we will propose an enhanced ACM by employing interval type-2 fuzzy sets to properly handle uncertainties in DIs. In particular, the following techniques are designed. (1) Fuzzy active contour models are enhanced into an interval type-2 fuzzy sets version for better discrimination between changed and unchanged regions in DIs in comparison to traditional fuzzy sets; different intermediate change detection masks are being generated by the designed interval type-2 fuzzy active contour model when it uses different combinations of fuzzy coefficients. (2) Each realization of the intermediate change detection mask has a cost value. The lower the cost value, the better the partition. A genetic algorithm (GA) approach is employed to find the final change detection mask by evolving the realization of intermediate change detection masks. Experimental results demonstrate good performance of the designed change detection approach for SAR images.

The rest of this paper is organized as follows. In Section 2, our motivation and main ideas concerning the proposed techniques are discussed. Section 3 describes the proposed algorithm in detail. In Section 4, experimental results on real multitemporal SAR images are described to demonstrate the effectiveness of the proposed approach. Conclusions are drawn in Section 5.

2. Motivation

Let us consider two coregistered SAR images, $I_1 = \{I_1(x, y), 1 \le x \le A, 1 \le y \le B\}$ and $I_2 = \{I_2(x, y), 1 \le x \le A, 1 \le y \le B\}$, both of size $A \times B$, acquired by a SAR sensor over the same geographical area at two different times. In order to suppress the effect of speckle noise, the probabilistic-patch-based (PPB) algorithm [38] is used to preprocess two coregistered SAR images. Log-ratio operator is then applied to two coregistered SAR images to generate a DI, $I_X = \{I_X(x, y), 1 \le x \le A, 1 \le y \le B\}$. Our objective is to design a binary classification technique to analyze the DI and produce a binary mask corresponding to changed and unchanged regions.

2.1. Motivation of Introducing Interval Type-2 Fuzzy Sets. Traditional energy function-based segmentation algorithms such as ACMs are designed by minimizing the distance between pixels and corresponding prototypes for dividing an image into distinct regions. ACMs are often called piecewise-constant models, since they are designed on the assumption that images are approximated by regions with piecewise-constant intensities. If a DI consists of nonoverlapping

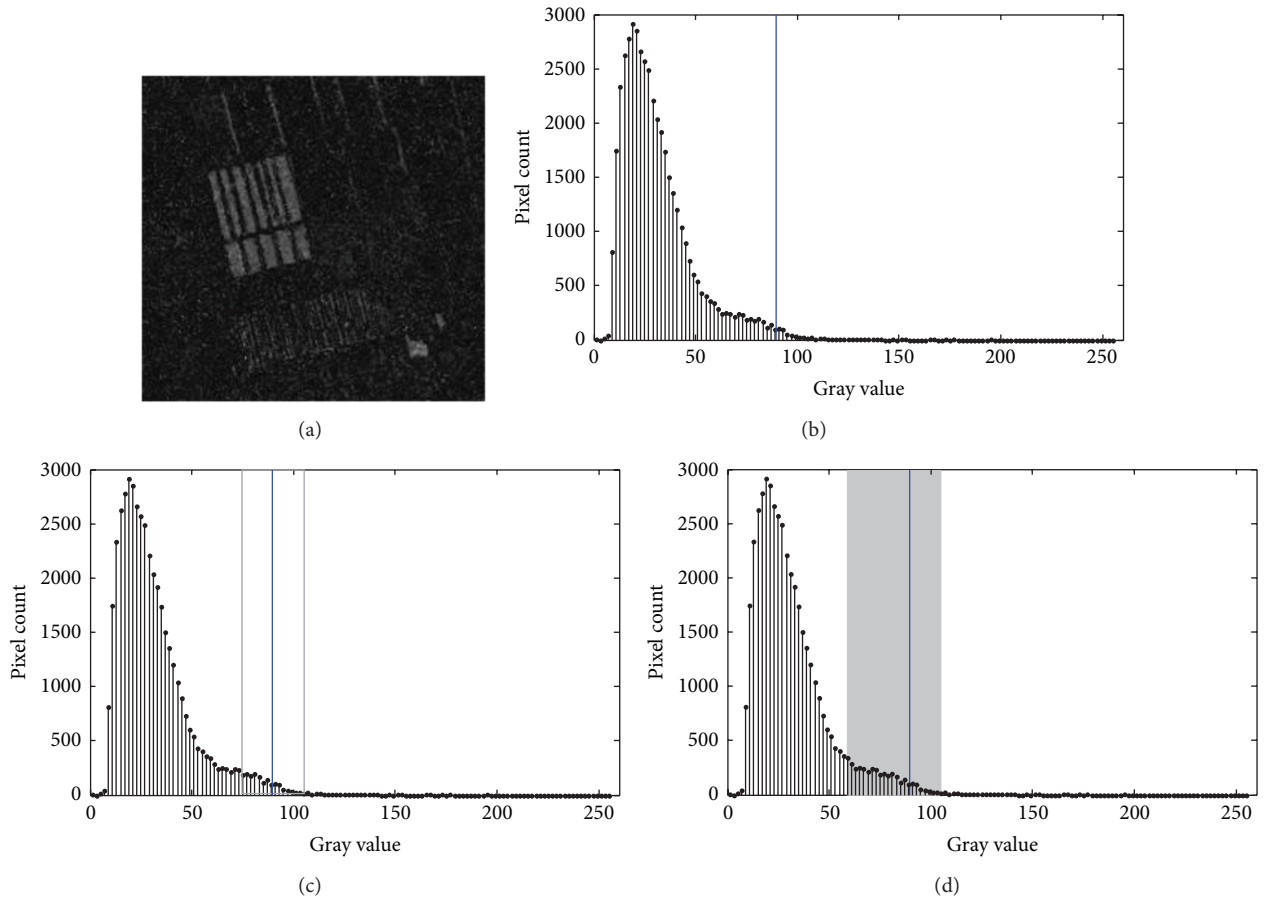

Figure 1: Example illustrating the variation of fuzzy region. (a) A DI sample, (b) decision boundary of the changed and unchanged regions, (c) fuzzy region for the changed and unchanged regions by a large fuzzifier m, and (d) desirable fuzzy region for the changed and unchanged regions.

regions, desirable change detection results can be obtained by traditional ACMs. However, in real applications, SAR images for which the DI has this property may be seldom encountered. The intensities of pixels belonging to changed and unchanged regions generally have overlapping region. In this case, fuzzy techniques which introduce the idea of partial membership by using membership degrees are more appropriate and realistic for describing uncertainties in real SAR images than hard techniques. The membership degree which reflects the degree of a pixel belonging to a certain region is computed as follows:

$$u(x,y) = \frac{1}{1 + \left(\left(I(x,y) - c_1 \right)^2 / \left(I(x,y) - c_2 \right)^2 \right)^{1/(m-1)}}, \tag{1}$$

$$c_1 = \frac{\int_\Omega \left[u(x,y) \right]^m I(x,y)\, dxdy}{\int_\Omega \left[u(x,y) \right]^m dxdy},$$
$$c_2 = \frac{\int_\Omega \left[1 - u(x,y) \right]^m I(x,y)\, dxdy}{\int_\Omega \left[1 - u(x,y) \right]^m dxdy}, \tag{2}$$

where c_1 and c_2 are the prototypes of changed and unchanged regions, respectively, m is the fuzzy coefficient, $I(x, y)$ is the gray value of the pixel located at (x, y) in the image domain Ω, and $u(x, y)$ represents the membership degree of pixel (x, y) belonging to changed region.

According to (1), membership degrees are calculated depending on the relative distance between a pixel and prototypes, as well as on the fuzzy coefficient. The membership degree $u(x, y)$ from (1) is a precise numeric value. This poses a dilemma of excessive precision in describing uncertain phenomenon. Thus we prefer to view membership degrees as uncertain values rather than, like in traditional fuzzy sets, as certain values. Figure 1 shows an example illustrating the rationality of creating uncertainty membership degrees. Figure 1(b) shows the gray histogram of the DI sample shown in Figure 1(a). The maximal fuzzy membership locations coincide with where patterns are equally distant from two prototypes. The blue vertical line denotes the position where pixels have equal distance from two prototypes, which can be taken as a decision boundary. In Figure 1(b), some pixels on the left side of the decision boundary, being part of the unchanged region, intuitively contribute more to the changed region than to the unchanged region, which may cause pixels within the changed region with similar intensity as the

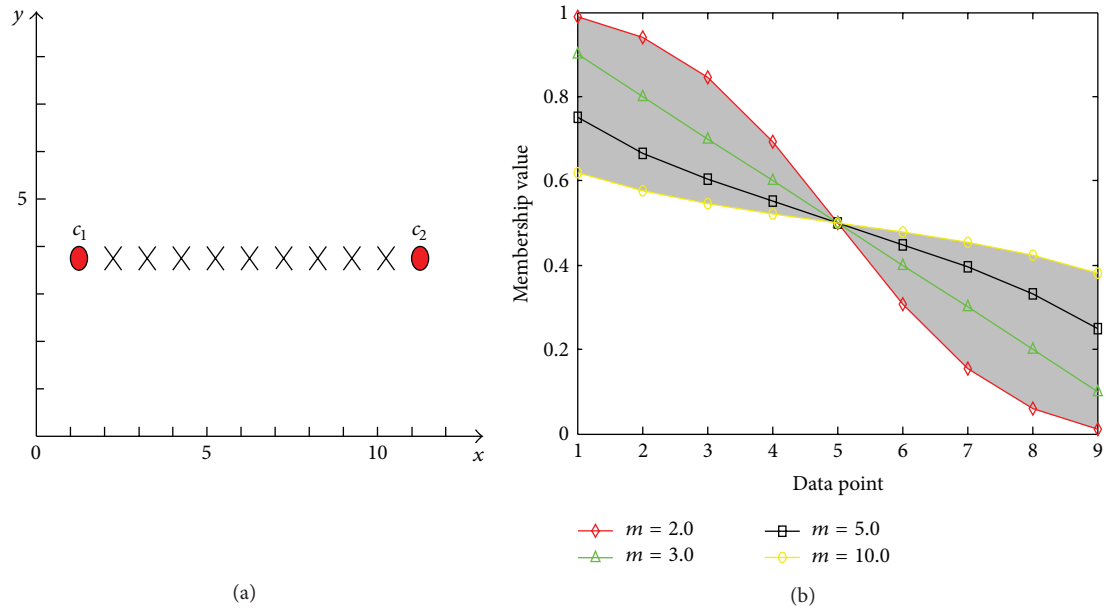

FIGURE 2: Example illustrating the variation of membership degrees. (a) Pattern set consisting of two prototypes. (b) Membership degrees for patterns located between c_1 and c_2 (from left to right) belonging to c_1 with various values of m.

unchanged region is difficult to be detected. Due to speckle noises, some unchanged pixels will be wrongly partitioned into changed region.

The crisp decision boundary should itself be considered as an uncertain fuzzy region. The width of the decision boundary (around the blue vertical line) indicates the range where one wants to assign maximal uncertainty to pixels. A larger value of m corresponds to a wider fuzzy boundary as shown in Figure 1(c), the gray rectangle, which can be taken as the maximal fuzzy region. It is more desirable to obtain a fuzzy region with wide left region and narrow right region as shown in Figure 1(d). Unfortunately, such desirable fuzzy region cannot be represented by any single m, since the change of m affects two sides of decision boundary equally. This suggests that a more appropriate way of fuzzy coefficients control is needed for improving segmentation results.

Interval type-2 fuzzy sets which adopt a secondary membership to define the possibilities of the primary membership provide a possible way to build such an uncertain fuzzy region. Due to the additional degree of freedom, interval type-2 fuzzy sets have shown better performance in modeling various uncertainties that cannot be appropriately managed by traditional fuzzy sets. In particular, an interval type-2 fuzzy approach is employed for creating uncertain membership degrees by using two fuzzy coefficients. The details of the proposed interval type-2 fuzzy approach for change detection will be presented in Section 3.1.

2.2. Motivation of Employing Genetic Algorithms. As analyzed in Section 2.1, membership degrees should be taken as uncertainty rather than as certainty, and the computation of membership degrees should not necessarily rely on a single fuzzy coefficient. Interval type-2 fuzzy sets can generate uncertain membership degrees by using two fuzzy coefficients. However, proper selection of fuzzy coefficients is a characteristic and unavoidable problem of interval type-2 fuzzy set-based algorithms.

Suppose that c_1 and c_2 are two prototypes of a pattern set shown in Figure 2(a). The plots of membership degrees corresponding to nine points belonging to prototype c_1 with various fuzzy coefficients are shown in Figure 2(b). The gray region is the footprint of uncertainty (FOU) of membership degrees [33]. Figure 2(b) shows that the FOU varies with different combinations of fuzzy coefficients. When the difference between fuzzy coefficients becomes larger, the size of FOU is enlarged, which increases the degree of freedom on modeling uncertainties. However, the increase of difference between fuzzy coefficients also brings potential problems. For image segmentation, the object boundary cannot be accurately described when the difference between fuzzy coefficients is too large. Thus, the selection of fuzzy coefficients has a great impact on segmentation results.

Since interval type-2 fuzzy set-based algorithms use different combinations of fuzzy coefficients, they will produce different change detection masks. The set of pixels which have different classification results among various change detection masks constitutes the difference region. Suppose that the number of pixels within the difference region is L; then there are 2^L possible combinations for pixels within the difference region. Each realization of a possible combination has a cost value. One of the 2^L possible combinations with the minimum cost value can be taken as the best change detection mask. Thus, we can avoid the problem of selecting fuzzy coefficients by finding the optimal combination of pixels within the difference region.

An exhaustive way for finding the best change detection mask is to compute the cost value of all 2^L possible combinations. In view of change detection on real SAR images, however, this approach is unfeasible, as the computation effort

takes far too long. But genetic algorithms (GAs), a heuristic stochastic search method inspired by the theory of natural evolution, offer a solution here. In GAs, a set of randomly generated chromosomes is evolved during certain generations. Evolution operators are performed through natural exchange of genetic material among chromosomes, which simulate the process of selection, crossover, and mutation. Chromosomes are evaluated via fitness functions which measure the fitness of a chromosome to survive. A GA will seek the optimal solution that maximizes or minimizes a fitness function. Our approach presents an unsupervised change detection approach for synthetic aperture radar images analysis. The GA approaches have already been introduced for solving the change detection task for SAR images [39–42]. In view of the many combinations possible, we try to employ a GA approach to find an optimal combination of pixels within the difference region.

3. Methodology

3.1. The Framework of the Proposed Change Detection Method. In this paper, our emphasis is on the analysis of DIs. The analysis step can be taken as the process of image segmentation. Figure 3 shows the framework of the proposed unsupervised distribution-free change detection approach which is made up of two main steps: (1) preliminarily analyze DIs by the designed interval type-2 fuzzy active contour model and generate different intermediate change detection masks; (2) finally employ a GA to evolve the realization of intermediate change detection masks for finding a final change detection mask. The proposed method is able to produce change detection results without any a priori assumption, which overcomes limitations arising from using statistical estimation models for changed and unchanged regions.

3.2. Extend the Active Contour Model to an Interval Type-2 Fuzzy Sets Version. As analyzed in Section 2.1, when using a single fuzzy coefficient it is difficult to obtain a satisfactory segmentation result in case the image is formed by overlapping regions. An interval type-2 fuzzy approach is employed to make membership degrees become uncertain. In particular, two fuzzy coefficients m_1 and m_2 are employed to generate two approximations of the membership degree. Let $m_2 > m_1$; the lower and upper membership degrees are calculated as follows:

$$\underline{u}(x,y) = \frac{1}{1+\left(\left(I(x,y)-v_1\right)^2/\left(I(x,y)-v_2\right)^2\right)^{1/(m_1-1)}},$$

$$\overline{u}(x,y) = \frac{1}{1+\left(\left(I(x,y)-v_1\right)^2/\left(I(x,y)-v_2\right)^2\right)^{1/(m_2-1)}}, \tag{3}$$

where v_1 and v_2 are the prototypes of the changed and unchanged regions, respectively, $I(x,y)$ is the gray value of the pixel located at (x,y), and $\underline{u}(x,y)$ and $\overline{u}(x,y)$ are two approximations of the membership degree of the pixel (x,y) belonging to the changed region.

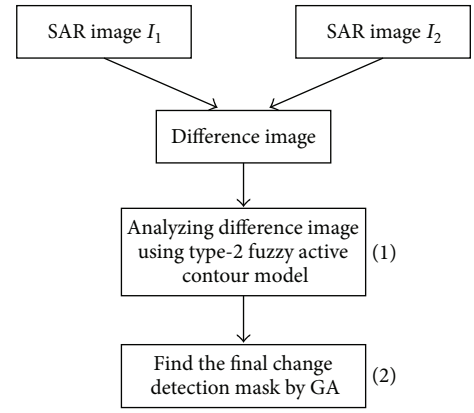

Figure 3: Framework of the proposed change detection approach.

Since we extend ACM into an interval type-2 fuzzy sets version, the uncertainty defined in interval type-2 fuzzy sets has to be managed appropriately through all steps of ACM, especially for the procedures of updating prototypes and defuzzification in the final decision. A type reduction procedure is necessary before we update prototypes and partition pixels in the final decision.

Since we use interval type-2 fuzzy sets to describe uncertainties, the membership degree of each pixel has lower and upper approximations. A type reduction for membership degrees is needed before we assign a pixel to the corresponding region, which is achieved as follows:

$$u_2(x,y) = \frac{\overline{u}(x,y) + \underline{u}(x,y)}{2}. \tag{4}$$

An iterative algorithm [43] is employed as a type reduction procedure for estimating the left and right values of a prototype. The procedure of calculating the right value of v_1 by the iterative algorithm is described as follows.

Step 1. Calculate membership degrees of each pixel through (3) and (4).

Step 2. Calculate the prototype c_1 through (2) by using membership degrees established in Step 1.

Step 3. Sort pixels in terms of gray value in ascending order and find the pixel with index k that has the minimum distance from c_1 among all the pixels. The membership degree of any pixel with index smaller than k $(i < k)$ is set equal to its lower membership degree; otherwise, the membership degree is set equal to its upper membership degree.

Step 4. Calculate the right value of the prototype c_{1r} through (2) by using membership degrees got in Step 3.

Step 5. If $c_{1r} = c_1$, stop; otherwise, set $c_1 = c_{1r}$ and go to Step 3.

The left value of the prototype c_{1l} can be obtained by the above iterative procedure by only replacing $i < k$ with $i \geq k$ in Step 3.

Crisp prototypes are obtained by a defuzzification method carried out as follows:

$$v_i = \frac{c_{il} + c_{ir}}{2}, \quad i = 1 \text{ or } 2. \tag{5}$$

Assume that the DI is formed by the changed and unchanged regions. The changed region is represented by the region inside the contour boundary, while the unchanged region is represented by the region outside the contour boundary. The contour boundary of the changed region is iteratively evolved in image domain Ω based on the minimization of an enhanced fuzzy energy function defined as follows:

$$\begin{aligned} F(v_1, v_2, u_2) = &\int_\Omega \left(u_2(x,y)\right)^m \left(I(x,y) - v_1\right)^2 d_x d_y \\ &+ \int_\Omega \left(1 - u_2(x,y)\right)^m \left(I(x,y) - v_2\right)^2 d_x d_y, \end{aligned} \tag{6}$$

where v_1 and v_2 are the prototypes of the changed and unchanged regions, respectively, $u_2(x, y)$ is the type-2 membership degree of the pixel (x, y) belonging to the changed region, m is the fuzzy coefficient, and $I(x, y)$ is the gray value of the pixel (x, y). The main steps of the proposed interval type-2 fuzzy active contour model for SAR image change detection are then presented as follows.

Step 1. Set parameters m, m_1, m_2, and ε and give an initial partition of the DI.

Step 2. Compute v_1 and v_2 using (5).

Step 3. Assume that the membership degree of current pixel is u_{2o}. Compute a new membership degree u_{2n} for the pixel according to (4). Compute the difference between the old and the new energy of each pixel as follows [17]:

$$\begin{aligned} \Delta F = &\left(u_{2n}^m - u_{2o}^m\right)\left(\frac{s_1}{s_1 + u_{2n}^m - u_{2o}^m}\right)\left(I_o - v_1\right)^2 \\ &+ \left(\left(1 - u_{2n}\right)^m - \left(1 - u_{2o}\right)^m\right) \\ &\times \left(\frac{s_2}{s_2 + \left(1 - u_{2n}\right)^m - \left(1 - u_{2o}\right)^m}\right)\left(I_o - v_2\right)^2, \end{aligned} \tag{7}$$

where $s_1 = \sum_\Omega [u_2(x, y)]^m$ and $s_2 = \sum_\Omega [1 - u_2(x, y)]^m$. If $\Delta F < 0$, u_{2o} is replaced by u_{2n}; else keep the old (u_{2o}) one.

Step 4. Compute the total energy according to (6). If F remains unchanged, stop. Otherwise, go to Step 2.

3.3. Employ a Genetic Algorithm to Find the Final Change Detection Mask. Since interval type-2 fuzzy set-based algorithms use different combinations of fuzzy coefficients, they will produce different intermediate change detection masks. The selection of fuzzy coefficients has a great impact on final results and requires a careful consideration in practical applications. In view of the many combinations possible, we try to avoid the problem of selecting fuzzy coefficients by using a GA approach.

Let us consider two intermediate change detection masks. M_1 and M_2 are generated by the proposed interval type-2 fuzzy active contour model with different fuzzy coefficients, respectively. Consider $M_1 = \{ms_1(x, y), 1 \le x \le A, 1 \le y \le B\}$ and $M_2 = \{ms_2(x, y), 1 \le x \le A, 1 \le y \le B\}$, where $ms_1(x, y) \in \{0, 1\}$ and $ms_2(x, y) \in \{0, 1\}$. The pixel value at spatial location (x, y) of an intermediate change detection mask is 0 when the corresponding pixel is predicted as changed and 1 when it is predicted as unchanged. The set of pixels which have different classification results among different intermediate change detection masks forms a difference region (DR $= \{(x, y) \mid ms_1(x, y) \neq ms_2(x, y)\}$). The set of pixels which have same classification results among different intermediate change detection masks forms a common region (CR $= \{(x, y) \mid ms_1(x, y) = ms_2(x, y)\}$). L is the number of pixels within the difference region. There are 2^L possible combinations for pixels within the difference region. Each realization of 2^L possible combinations has a cost function value. One of the possible combinations has the minimum cost function value which can be selected as the optimum combination of pixels within DR. An exhaustive way for finding the optimal combination is computing all the possible combinations, which is rather impossible for the task of change detection on real SAR images. The GA is employed to find the optimal combination of pixels within the difference region.

3.3.1. String Representation. In GAs, a fixed number of chromosomes form a population which is evolved toward better solutions. In our situation, a chromosome C is generated as a binary string of size L (where $C(i) \in \{0, 1\}$, $1 \le i \le L$) representing a possible combination for pixels within the difference region. The length of the chromosome equals the number of pixels within the difference region. If the pixel with index i is predicted as a changed pixel, the gene $C(i)$ of the chromosome is 0. Otherwise, the gene $C(i)$ of the chromosomeis 1.

3.3.2. Computing the Fitness Value. Each chromosome has a cost value which somehow measures the fitness of it to survive in the population. In our approach, the lower the cost value, the higher the probability for the corresponding chromosome to survive in the next generation. The cost function F is computed as follows [44]:

$$F = \sum_{r=0}^{1} \frac{N_r}{L} \sum_{\forall i \in R_r} \left(I_d(i) - \mu_r\right)^2 \tag{8}$$

$$\begin{aligned} &R_0 = \{i \mid C(i) = 0\}, \qquad R_1 = \{i \mid C(i) = 1\}, \\ &\mu_0 = \frac{1}{N_0} \sum_{\forall i \in R_0} I_d(i), \qquad \mu_1 = \frac{1}{N_1} \sum_{\forall i \in R_1} I_d(i), \end{aligned} \tag{9}$$

where R_0 and R_1 denote the sets of changed and unchanged pixels, respectively, represented by the chromosome C, L is the length of the chromosome, N_0 and N_1 are the number

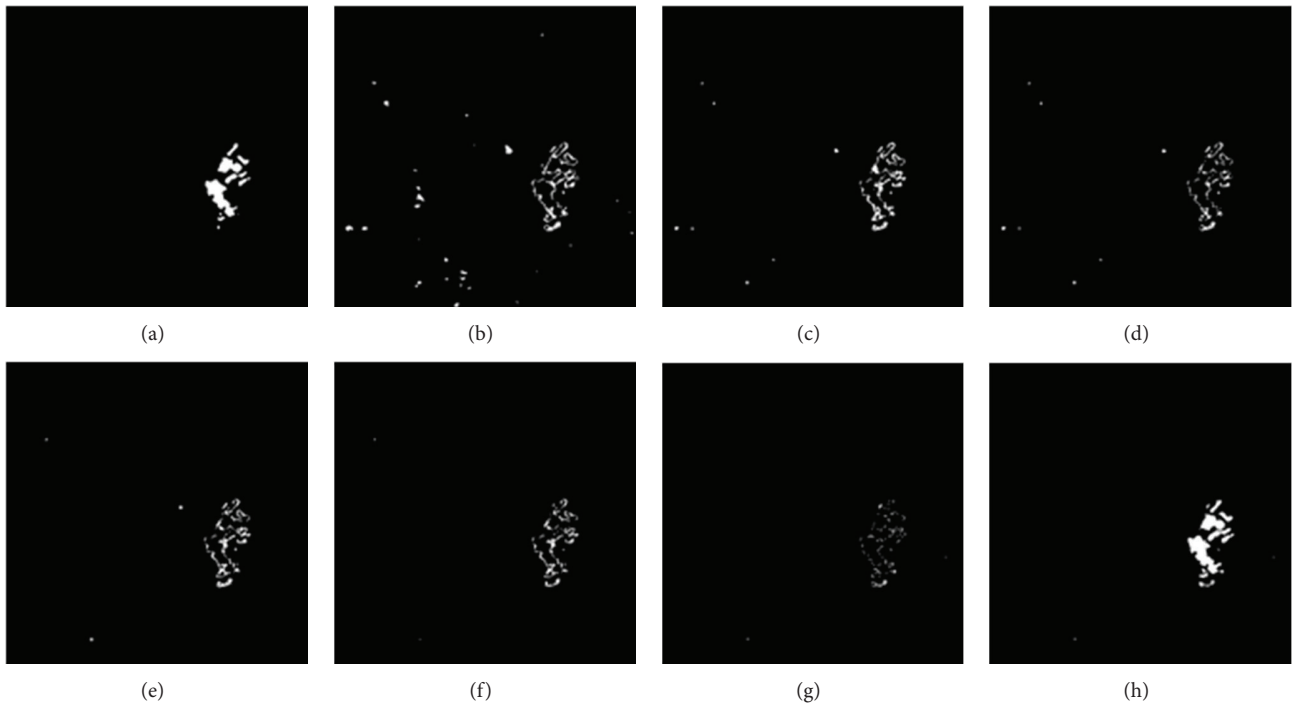

Figure 4: Intermediate evolution results at different numbers of function evaluations. (a) Pixels within the common region among different change detection masks. (b) Pixels within the difference region among different change detection masks. (c) The evolution result of pixels within the difference region with 10,000 function evaluations. (d) The evolution result of pixels within the difference region with 20,000 function evaluations. (e) The evolution result of pixels within the difference region 30,000 function evaluations. (f) The evolution result of pixels within the difference region with 40,000 function evaluations. (g) The evolution result of pixels within the difference region with 50,000 function evaluations.

of pixels in R_0 and R_1, respectively, and I_d is the set of pixels selected from the DI which has the same index as the pixels within the difference region.

The weighted sum of the mean square error (MSE) of the changed and unchanged regions is used as a cost value for the corresponding combination of pixels within the difference region [44]. The lower the MSE, the better the partition. Equation (8) approaches to zero when a chromosome adequately partitions pixels within the difference region into changed and unchanged regions.

3.3.3. Genetic Operators. The population of the next generation is formed by using a probabilistic reproduction process. Chromosomes with higher fitness have a larger contribution to the generation of offspring. Selection schemes are used to select good chromosomes according to their fitness to breed a new generation. The selection schemes such as proportional, ranking and tournament rule are widely used in GAs. The resulting population after selection is called the intermediate population. The intermediate population is evolved by using crossover and mutation to form the next generation. In this work, we employ the ranking rule as a selection scheme followed by the conventional two-point crossover and uniform mutation. Commonly, a GA terminates when a maximum number of function evaluations have been reached, and 50,000 function evaluations are used as a stop criterion in this work.

The intermediate evolution results of pixels within the difference region with different numbers of function evaluations are shown in Figure 4. Pixels within the common region among different change detection masks are shown in Figure 4(a). An initial chromosome which presents a possible combination of pixels within the difference region is shown in Figure 4(b). Chromosomes are iteratively refined as shown in Figures 4(b)–4(g) to obtain the optimum combination as shown in Figure 4(g). Figure 4(h) shows the final change detection mask which is obtained by the combination of Figures 4(a) and 4(g).

4. Experimental Results

In this section, we will evaluate the performance of the proposed method on three SAR datasets. The preprocess typical corrections, such as topographic correction, geometric correction, and atmospheric correction, have been done on images before we apply the proposed method. A log-ratio operator is employed to generate DIs. A classical threshold selection method (OTSU) [45] is employed for comparative analysis. A fuzzy local information c-means clustering algorithm (FLICM) [27] being a progressive clustering algorithm is employed. Since the proposed method is originated from active contour methodology, three ACMs including the Chan-Vese (CV) [13] model, the distance regularized level set evolution model (DRLSE) [19], and fuzzy energy-based active

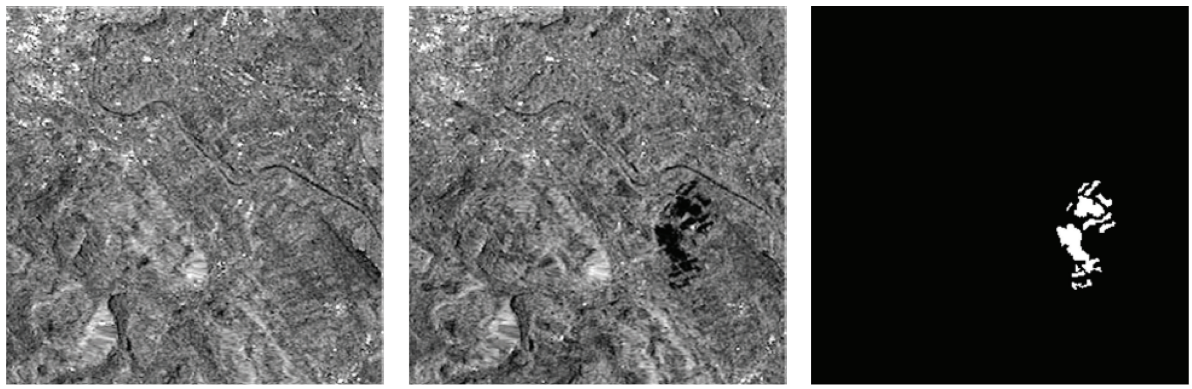

(a) (b) (c)

Figure 5: Bern dataset. (a) Image acquired in April 1999. (b) Image acquired in May 1999. (c) Ground truth image.

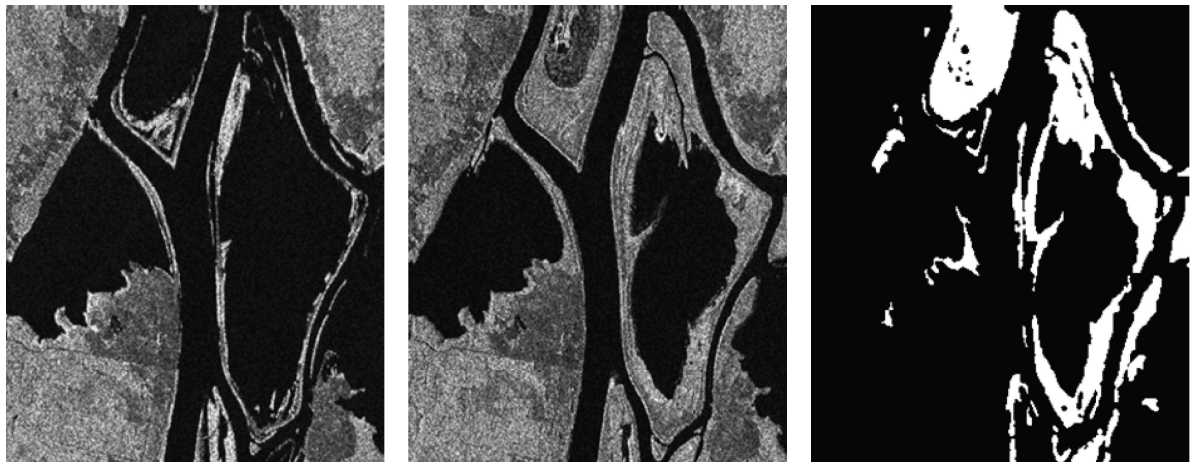

(a) (b) (c)

Figure 6: Ottawa dataset. (a) Image acquired in April 1999. (b) Image acquired in May 1999. (c) Ground truth image.

contour model (FAC) [17] are employed for comparative analysis. We present comparative analysis of the proposed method with the state-of-art methods including OTSU, FLICM, CV, DRLSE, and FAC. In our proposed method, the threshold $\varepsilon = 10^{-4}$ is used as a stopping condition, and the fuzzy factor m took its default value 2.

4.1. Datasets. In order to validate the performance of the compared methods, three SAR image datasets with different characteristics are used in the experiments. The first dataset is the Bern dataset, which presents a section (301 × 301) of two SAR images acquired by the European Remote Sensing 2 satellite SAR sensor of an area near the city of Bern, Switzerland, in April and May 1999, respectively. Between the two dates, River Aare flooded parts of the cities of Thun and Bern and the airport of Bern entirely. Hence, the Aare valley between Bern and Thun was selected as a test site for detecting flooded areas. The images and the available ground truth which is obtained by integrating a priori information with photo interpretation are shown in Figure 5.

The second dataset is a section (290 × 350 pixels) of two SAR images of the city of Ottawa acquired by RADARSAT SAR sensor. They were provided by Defense Research and Development Canada (DRDC), Ottawa. Figure 6(a) shows the image acquired in May 1997 during the summer flooding and Figure 6(b) shows the image acquired in August 1997 after the summer flooding. This dataset presents the areas where they were once afflicted with floods. The available ground truth which is created by integrating a priori information with photo interpretation is shown in Figure 6(c).

The third dataset comes from two SAR images acquired by Radarsat-2 at the region of Yellow River Estuary in China in June 2008 and June 2009, respectively. The original SAR images acquired by Radarsat-2 are shown in Figures 7(a) and 7(b) with the size of 7666 × 7692. They are too huge to detail the information for our purposes, so a small typical area of size 306 × 291 pixels is selected to compare the change detection results of different approaches. The selected images and the available ground truth which is created by integrating a priori information with photo interpretation are shown in Figure 7. It should be noted that both images considered are a

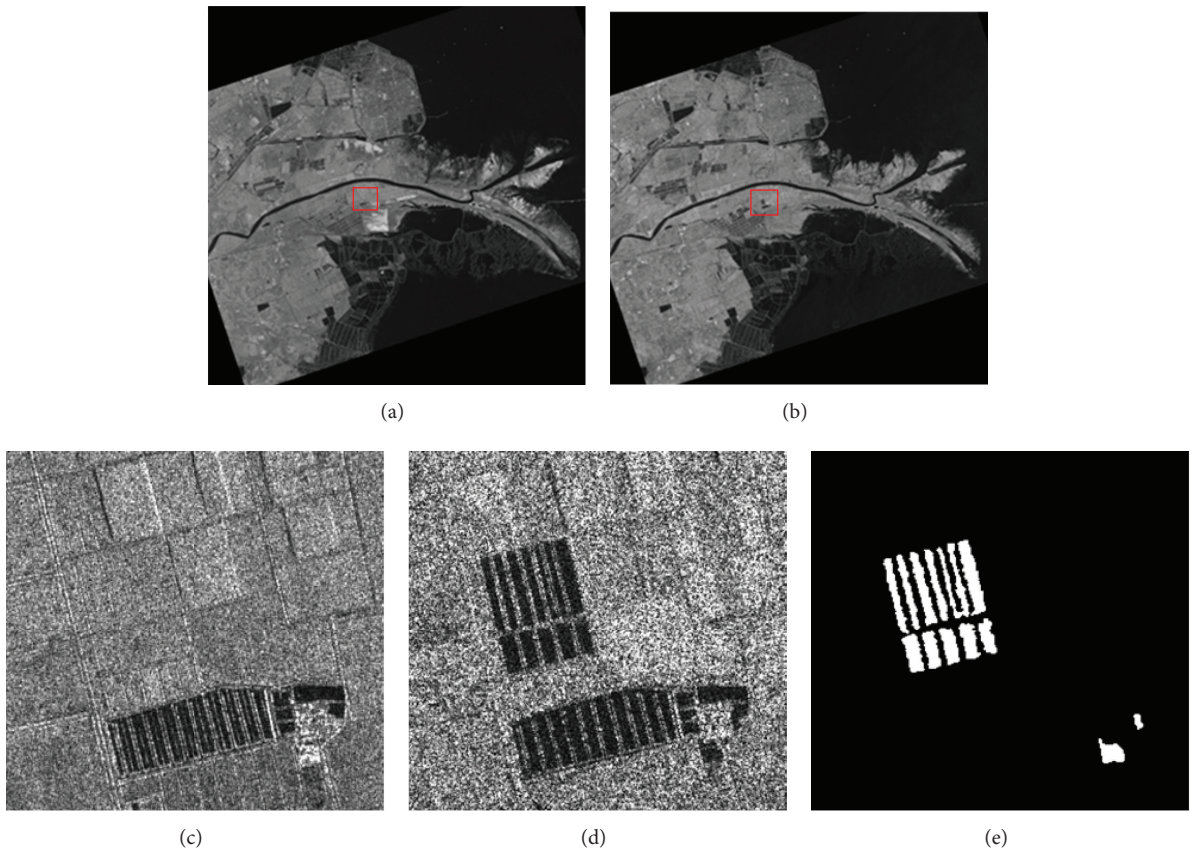

FIGURE 7: Yellow River dataset. (a) Image acquired in June 2008. (b) Image acquired in June 2009. (c) Image of the representative area acquired in June 2008. (d) Image of the representative area acquired in June 2009. (e) Ground truth image.

single-look image and a four-look image, respectively. Thus, the influence of speckle noise on the image acquired in 2009 is much greater than the one acquired in 2008. So it represents a more complicated situation for change detection, due to the difference of speckle noise level between the two images.

4.2. The Effect of GA Parameters and Fuzzy Coefficients. The influence of GA parameters and fuzzy coefficients are discussed in this part. We first analyze the role of fuzzy coefficients on the generation of intermediate change detection masks. As shown in Figure 2, the difference between two fuzzy coefficients controls the size of FOU. To get very different intermediate change detection masks, we want to choose two quite different combinations of fuzzy coefficients which form a small FOU and a large FOU, respectively. The selection of fuzzy coefficients is analyzed as follows.

Figure 8 shows intermediate change detection masks on the Bern dataset obtained by the proposed interval type-2 fuzzy active contour model with different combinations of fuzzy coefficients. It can be seen that results are unsatisfying when the difference between m_1 and m_2 is small. Figure 8(a) shows that only the explicit changed pixels can be detected. When the difference between m_1 and m_2 becomes larger, the FOU of membership degrees will be enlarged, which increases the degree of freedom on modeling uncertainties. In this case, even the changed pixels with little difference from the background can be detected. However, the increase of the difference between m_1 and m_2 also brings a potential problem. Due to speckle noises, some unchanged pixels are wrongly partitioned into changed region, and the boundary of changed region cannot be well described as shown in Figures 8(h)–8(j). Therefore, we choose two combinations of fuzzy coefficients with a small uncertainty region ($m_1 = 1.1$ and $m_2 = 2$) and a large uncertainty region ($m_1 = 1.1$ and $m_2 = 11$), respectively, in order to get very different intermediate change detection masks.

In the below experiments, we analyze the influence of GA parameters. For demonstration purposes, the minimum cost function value of the population with different numbers of function evaluations on the Bern dataset has been computed for different GA parameters. GA parameters analysis results are demonstrated in Figure 9. Figure 9(a) shows the performance of crossover operator using a different crossover rate. It demonstrates that the higher the crossover rate, the lower the cost function value. The effect of mutation rate is shown in Figure 9(b). In contrast to the crossover rate, keeping the mutation rate high will increase the cost function value. It has been empirically found that GA parameter settings with $m_r = 0.01$ and $c_r = 0.8$ provide most satisfactory results.

4.3. Segmentation Accuracy Assessment. In order to provide the quantitative analysis of the compared methods, the

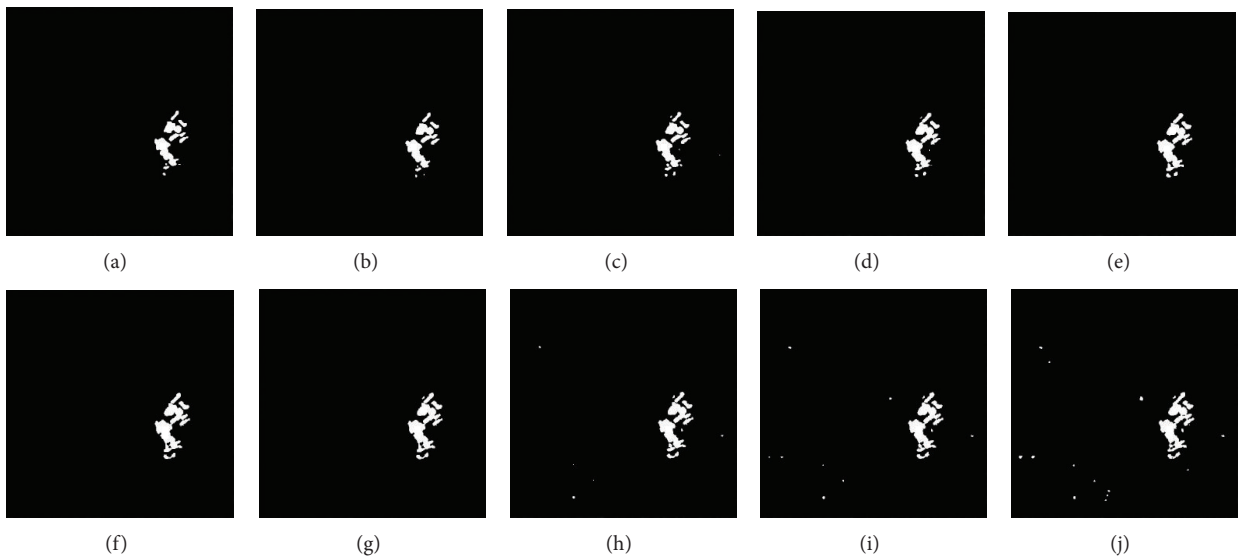

FIGURE 8: Segmentation result on a difference image with the differences between m_1 and m_2 from 1 to 10 with an interval of 1 shown in (a) to (j).

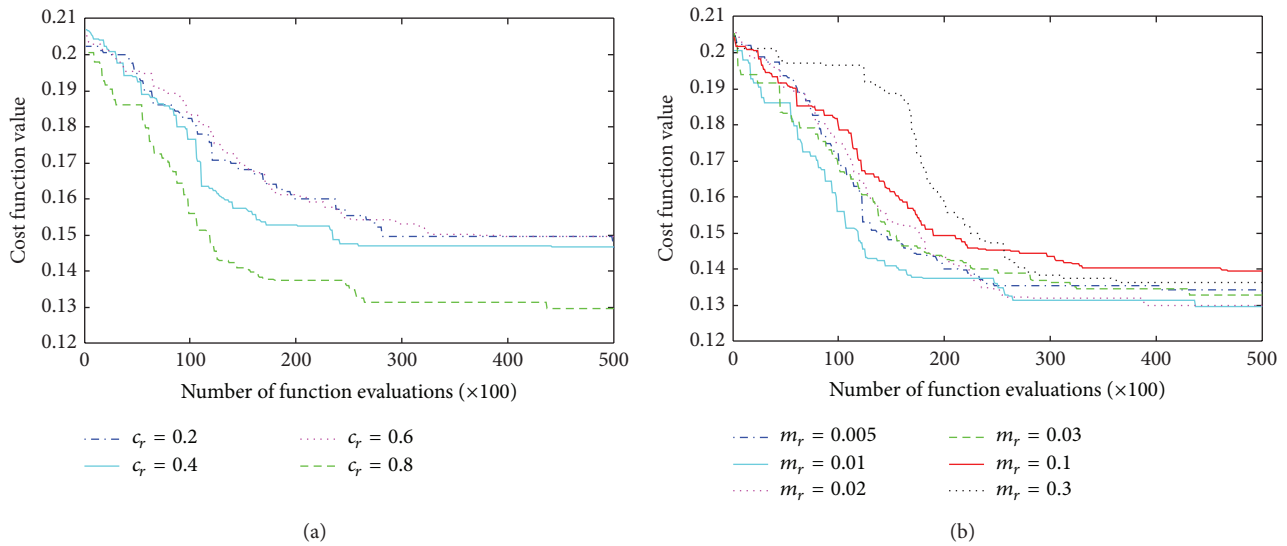

FIGURE 9: The performance of the proposed method under different GA parameters on the Bern dataset. (a) The performance with respect to different crossover rate with $m_r = 0.01$. (b) The performance with respect to different mutation rate with $c_r = 0.8$.

following measures [46] are computed for change detection results. True positive (TP) is the number of pixels that are detected as the changed area both in the reference image and in the change detection result. True negative (TN) is the number of pixels that are detected as the unchanged area both in the reference image and in the change detection result. False negative (FN) is the number of pixels that are detected as changed area in the reference image and as unchanged area in the change detection result. False positive (FP) is number of pixels that are detected as unchanged area in the reference image and as changed area in the change detection result. Overall error (OE) is the total number of decision errors which equals the sum of FN and FP. The percentage correct classification (PCC) is calculated as follows:

$$\text{PCC} = \frac{\text{TP} + \text{TN}}{\text{TP} + \text{TN} + \text{FP} + \text{FN}}. \tag{10}$$

In addition, Kappa statistic taking into account commission and omission errors is employed for evaluating the performance comparison of the methods. Kappa statisticis calculated as follows:

$$\text{Kappa} = \frac{\text{PCC} - \text{PRE}}{1 - \text{PRE}}, \tag{11}$$

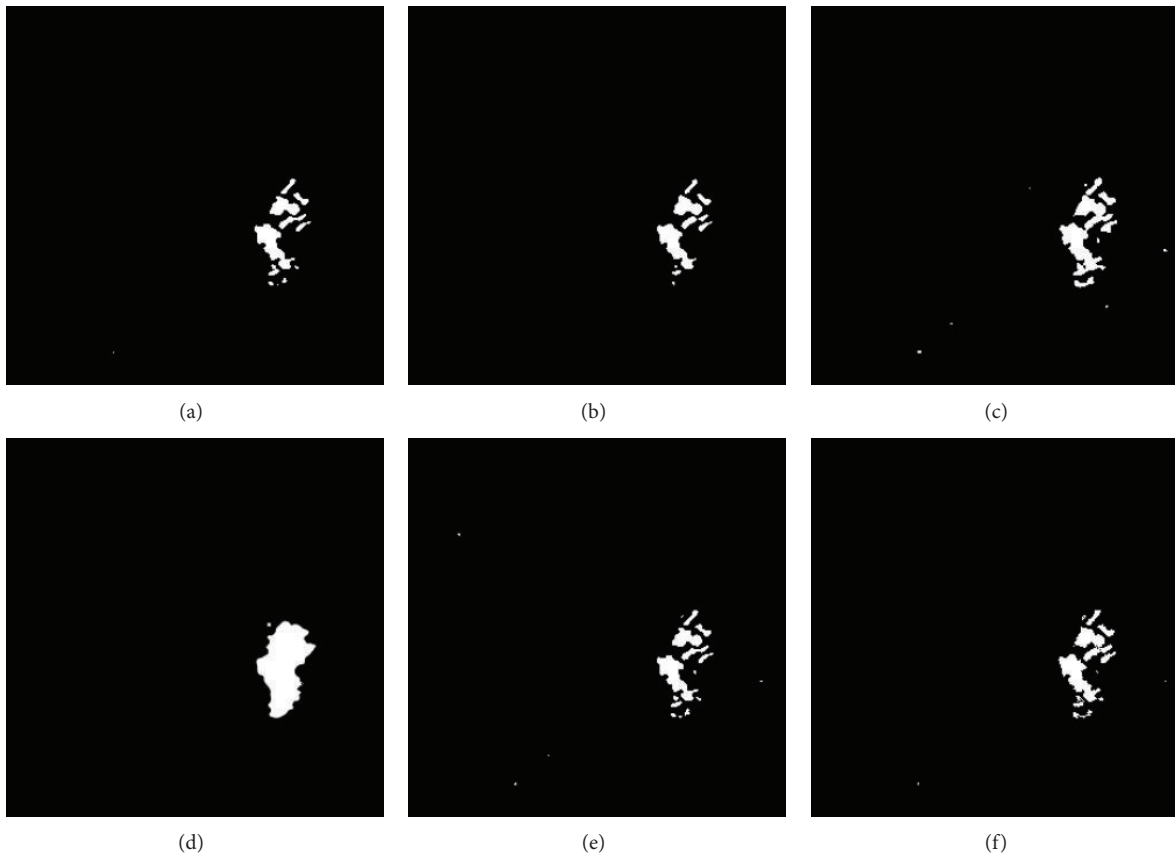

Figure 10: The final results of the Bern dataset generated by (a) OTSU, (b) FLICM, (c) CV, (d) DRLSE, (e) FAC, and (f) the proposed method.

Table 1: Comparison of the change detection results on the Bern dataset obtained by different methods.

Method	OTSU	FLICM	CV	DRLSE	FAC	The proposed method
FP	63	37	240	1061	76	87
FN	250	285	113	114	249	140
PCC	99.65%	99.64%	99.61%	98.70%	99.64%	99.75%
OE	313	322	353	1175	325	227
Kappa	0.8508	0.8421	0.8532	0.6332	0.8461	0.8982

where PRE = ((TP + FP)(TP + FN) + (FN + TN)(TN + FP))/(TP + TN + FP + TN)^2.

If the change detection result and the reference image are in full agreement, the Kappa value is 1. If there is no agreement between the change detection result and the reference image, the Kappa value is 0.

4.4. Experimental Results

4.4.1. Results for the Bern Dataset. The final results of the methods comparison for the Bern dataset are demonstrated in Figure 10. According to Figure 10(a), the change detection result achieved by OTSU only detects changed region with distinct difference from unchanged region. By contrast, with the introducing of fuzzy logic, the change detection results generated by FLICM and FAC detect more changed pixels as shown inFigures 10(b) and 10(e), respectively. Figure 10(d) demonstrates that the DRLSE model cannot detect changed region with weak boundaries, since it relies on edge function to stop curve evolution. The result obtained by the CV model which uses the region-based energy function is better than that of the DRLSE model as can be seen from Figure 10(c). The comparison between Figures 10(e) and 10(f) demonstrates the effectiveness of introducing interval type-2 fuzzy sets which increases the ability to model uncertainties. The proposed method can detect more changed pixels than the FAC model. Even changed pixels with little difference from the background can be detected. Table 1 lists the results of Kappa, OE, PCC, FP, and FN obtained by different methods. From Table 1, we can see that FN and FP of the proposed method do not exhibit the best, whereas OE, PCC, and Kappa which can be taken as overall evaluations are the best compared to the other approaches.

4.4.2. Results for the Ottawa Dataset. The visual and quantitative results on the Ottawa dataset are shown in Figure 11 and

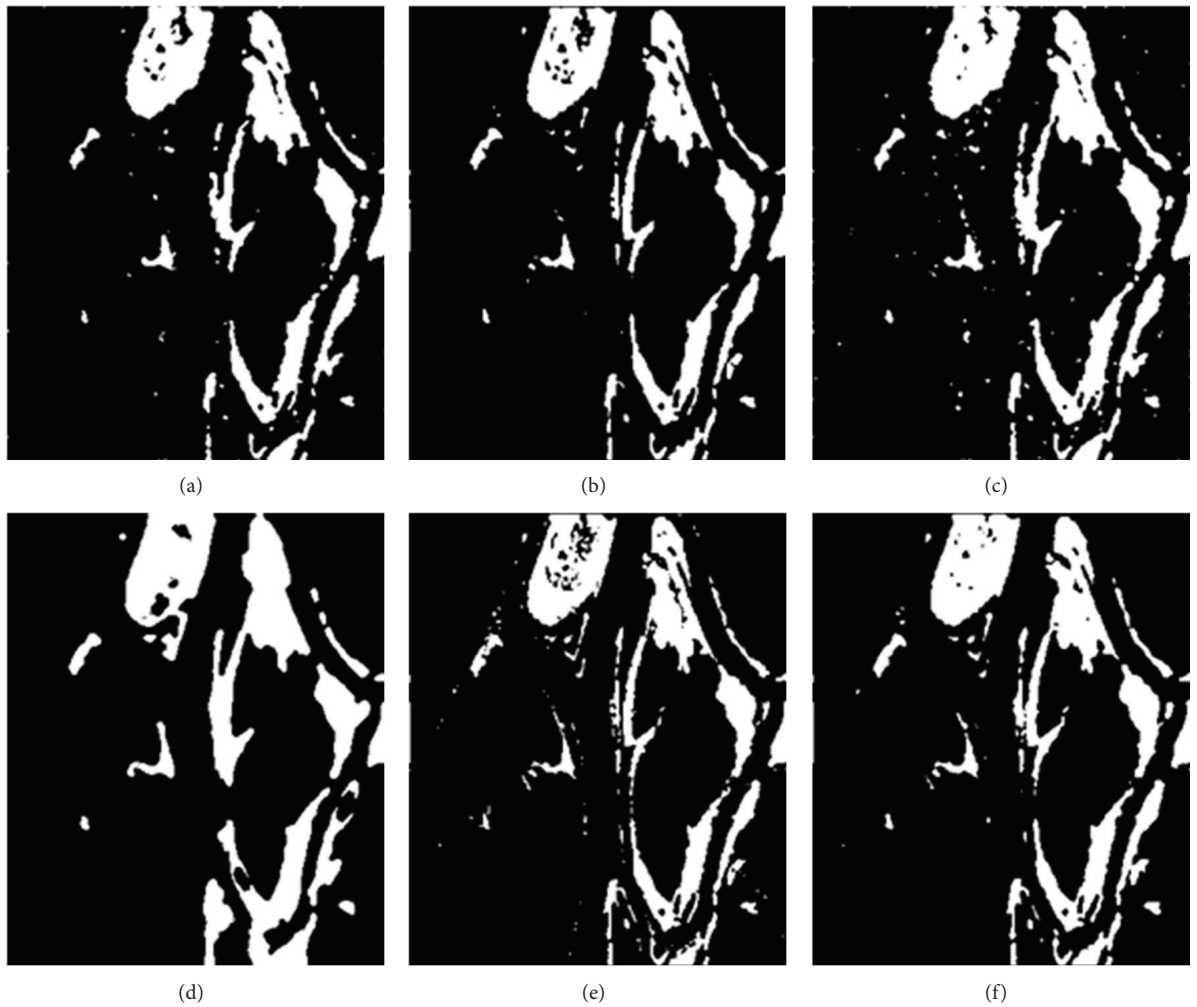

Figure 11: The final results of the Ottawa dataset generated by (a) OTSU, (b) FLICM, (c) CV, (d) DRLSE, (e) FAC, and (F) the proposed method.

Table 2: Comparison of the change detection results on the Ottawa dataset obtained by different methods.

Method	OTSU	FLICM	CV	DRLSE	FAC	The proposed method
FP	546	48	1397	3371	236	412
FN	2561	2406	1586	1257	2082	767
PCC	96.94%	97.58%	97.06%	95.44%	97.72%	98.84%
OE	3107	2454	2983	4628	2318	1179
Kappa	0.8790	0.9035	0.8892	0.8137	0.9101	0.9560

Table 2, respectively. The comparison analysis of Figures 11(c) and 11(e) shows that the change detection result obtained by the CV model is more sensitive to noise than those of the FAC model and FLICM. Such result is due to the fact that fuzzy energy functions used in FAC and FLICM provide a better ability to reject weak local minima than the hard version used in the CV model. Figure 11(d) shows that the result obtained by DRLSE is most insensitive to noise. However, the result of DRLSE is not good enough, as the boundary of changed region is not well depicted. The comparison between Figures 11(e) and 11(f) shows that even changed pixels with little difference from the background can be well detected by the proposed method. Considering the result shown in Table 2, the FN of the proposed method is much smaller than that of the FAC model. To sum up, the proposed method obtains the highest PCC and Kappa and the lowest OE of different methods as reported in Table 2.

4.4.3. Results for the Yellow River Dataset. The visual comparison between different change detection results is shown in Figure 12. There are many small noise spots in the change detection results of OTSU, FAC, and CV, while those of DRLSE, FLICM, and the proposed method possess much less

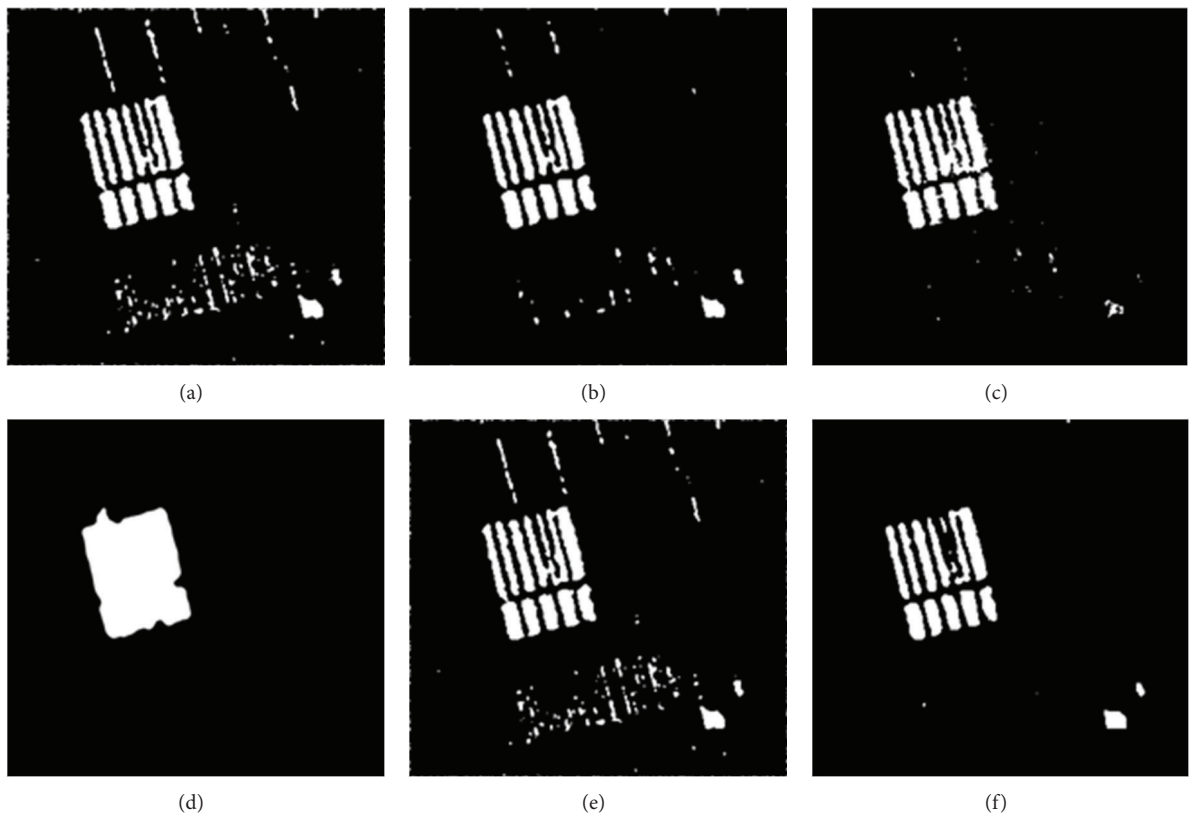

Figure 12: The final results of the selected area of the Yellow River dataset generated by (a) OTSU, (b) FLICM, (c) CV, (d) DRLSE, (e) FAC, and (f) the proposed method.

Table 3: Comparison of the change detection results on the Yellow River estuary dataset obtained by different methods.

Method	OTSU	FLICM	CV	DRLSE	FAC	The proposed method
FP	1862	605	316	2673	1759	263
FN	170	296	940	467	189	463
PCC	97.72%	98.99%	98.59%	96.47%	97.81%	99.18%
OE	2032	901	1256	3140	1948	726
Kappa	0.7965	0.8971	0.8462	0.6995	0.8028	0.9124

noise spots. DRLSE is most insensitive to noise. However, the changed detection result of the edge-based DRLSE model is not good enough. Due to using the gradient flow to stop curve evolution, DRLSE cannot identify the detail changes of the farmland area. Besides, many unchanged small areas are incorrect detected as changed by DRLSE. By comparison, the change detection results of FLICM and the proposed method can reflect real change trends as shown in Figures 12(b) and 12(f), respectively. Figure 12(f) shows that the change detection result provided by the propped method is very close to the ground truth. Moreover, as reported in Table 3, the proposed method obtains the lowest value of OE and the highest values of PCC and Kappa, which shows the effectiveness of the proposed method.

5. Concluding Remarks

In this paper, we have presented an unsupervised change detection approach towards the analysis of multitemporal SAR images. The proposed approach is based on an interval type-2 fuzzy active contour model and the genetic algorithm. Since interval type-2 fuzzy sets have a good adaptability to model various uncertainties which cannot be appropriately managed by traditional fuzzy sets, we extend active contour model to the interval type-2 fuzzy sets version for increasing the ability to handle inexact information in DIs. A proper selection of fuzzy coefficients is an unavoidable problem in interval type-2 fuzzy set-based algorithms. To overcome this problem, certain intermediate change detection masks are

generated by the proposed interval type-2 fuzzy active contour model when it uses different combinations of fuzzy coefficients. The GA is then employed to evolve the realization of intermediate change detection masks for finding the final change detection mask. Experimental results demonstrate that the proposed method gains a better performance on three real SAR datasets. It can robustly analyze DIs even in the presence of high intensity variation between changed and unchanged pixels, which is detrimental to traditional fuzzy active contour models.

Conflict of Interests

The authors declare that there is no conflict of interests regarding the publication of this paper.

Acknowledgments

This work was supported by the National Basic Research Program (973 Program) of China (no. 2013CB329402), the National Natural Science Foundation of China (Grant nos. 61377011, 61302063, 61273317, 61202176, and 61203303), the National Research Foundation for the Doctoral Program of Higher Education of China (no. 20100203120008), and the Fundamental Research Funds for the Central Universities (Grant nos. K5051302028 and K5051202053).

References

[1] J. Inglacla and G. Mercier, "A new statistical similarity measure for change detection in multitemporal SAR images and its extension to multiscale change analysis," *IEEE Transactions on Geoscience and Remote Sensing*, vol. 45, no. 5, pp. 1432–1445, 2007.

[2] S. Marchesi, F. Bovolo, and L. Bruzzone, "A context-sensitive technique robust to registration noise for change detection in VHR multispectral images," *IEEE Transactions on Image Processing*, vol. 19, no. 7, pp. 1877–1889, 2010.

[3] A. Robin, L. Moisan, and S. le Hegarat-Mascle, "An a-contrario approach for subpixel change detection in satellite imagery," *IEEE Transactions on Pattern Analysis and Machine Intelligence*, vol. 32, no. 11, pp. 1977–1993, 2010.

[4] M. Bosc, F. Heitz, J.-P. Armspach, I. Namer, D. Gounot, and L. Rumbach, "Automatic change detection in multimodal serial MRI: application to multiple sclerosis lesion evolution," *NeuroImage*, vol. 20, no. 2, pp. 643–656, 2003.

[5] D.-M. Tsai and S.-C. Lai, "Independent component analysis-based background subtraction for indoor surveillance," *IEEE Transactions on Image Processing*, vol. 18, no. 1, pp. 158–167, 2009.

[6] S.-S. Ho and H. Wechsler, "A martingale framework for detecting changes in data streams by testing exchangeability," *IEEE Transactions on Pattern Analysis and Machine Intelligence*, vol. 32, no. 12, pp. 2113–2127, 2010.

[7] L. Bruzzone and S. B. Serpico, "An iterative technique for the detection of land-cover transitions in multitemporal remote-sensing images," *IEEE Transactions on Geoscience and Remote Sensing*, vol. 35, no. 4, pp. 858–867, 1997.

[8] T. Hame, I. Heiler, and J. S. Miguel-Ayanz, "An unsupervised change detection and recognition system for forestry," *International Journal of Remote Sensing*, vol. 19, no. 6, pp. 1079–1099, 1998.

[9] G. di Martino, A. Iodice, D. Riccio, and G. Ruello, "A novel approach for disaster monitoring: fractal models and tools," *IEEE Transactions on Geoscience and Remote Sensing*, vol. 45, no. 6, pp. 1559–1570, 2007.

[10] M. K. Ridd and J. Liu, "A comparison of four algorithms for change detection in an urban environment," *Remote Sensing of Environment*, vol. 63, no. 2, pp. 95–100, 1998.

[11] J. Wu, A. Paul, Y. Xing et al., "Morphological dilation image coding with context weights prediction," *Signal Processing: Image Communication*, vol. 25, no. 10, pp. 717–728, 2010.

[12] M. Kass, A. Witkin, and D. Terzopoulos, "Snakes: active contour models," *International Journal of Computer Vision*, vol. 1, no. 4, pp. 321–331, 1988.

[13] T. F. Chan and L. A. Vese, "Active contours without edges," *IEEE Transactions on Image Processing*, vol. 10, no. 2, pp. 266–277, 2001.

[14] C. Li, R. Huang, Z. Ding, J. C. Gatenby, D. N. Metaxas, and J. C. Gore, "A level set method for image segmentation in the presence of intensity inhomogeneities with application to MRI," *IEEE Transactions on Image Processing*, vol. 20, no. 7, pp. 2007–2016, 2011.

[15] A. Paul, J. Wu, J.-F. Yang, and J. Jeong, "Gradient-based edge detection for motion estimation in H.264/AVC," *IET Image Processing*, vol. 5, no. 4, pp. 323–327, 2011.

[16] T. N. A. Nguyen, J.-F. Cai, J.-Y. Zhang, and J.-M. Zheng, "Robust interactive image segmentation using convex active contours," *IEEE Transactions on Image Processing*, vol. 21, no. 8, pp. 3734–3743, 2012.

[17] S. Krinidis and V. Chatzis, "Fuzzy energy-based active contours," *IEEE Transactions on Image Processing*, vol. 18, no. 12, pp. 2747–2755, 2009.

[18] Y.-G. Liu and Y.-Z. Yu, "Interactive image segmentation based on level sets of probabilities," *IEEE Transactions on Visualization and Computer Graphics*, vol. 18, no. 2, pp. 202–213, 2012.

[19] C. Li, C.-Y. Xu, C.-F. Gui, and M. D. Fox, "Distance regularized level set evolution and its application to image segmentation," *IEEE Transactions on Image Processing*, vol. 19, no. 12, pp. 3243–3254, 2010.

[20] C. Li, C. Xu, C. Gui, and M. D. Fox, "Level set evolution without re-initialization: a new variational formulation," in *Proceedings of the IEEE Computer Society Conference on Computer Vision and Pattern Recognition (CVPR '05)*, pp. 430–436, San Diego, Calif, USA, June 2005.

[21] K. Zhang, L. Zhang, H. Song, and W. Zhou, "Active contours with selective local or global segmentation: a new formulation and level set method," *Image and Vision Computing*, vol. 28, no. 4, pp. 668–676, 2010.

[22] J. Ning, L. Zhang, D. Zhang, and C. Wu, "Interactive image segmentation by maximal similarity based region merging," *Pattern Recognition*, vol. 43, no. 2, pp. 445–456, 2010.

[23] K. Zhang, H. Song, and L. Zhang, "Active contours driven by local image fitting energy," *Pattern Recognition*, vol. 43, no. 4, pp. 1199–1206, 2010.

[24] G. Yin, S. Wang, and X. Jin, "Optimal slip ratio based fuzzy control of acceleration slip regulation for four-wheel independent driving electric vehicles," *Mathematical Problems in Engineering*, vol. 2013, Article ID 410864, 7 pages, 2013.

[25] T. Allahviranloo, R. R. Yager, S. Abbasbandy, and G. Ulutagay, "Ranking fuzzy numbers and its extensions," *Mathematical Problems in Engineering*, vol. 2013, Article ID 468635, 1 page, 2013.

[26] C. Monteiro, L. A. Fernandez-Jimenez, I. J. Ramirez-Rosado, A. Muñoz-Jimenez, and P. M. Lara-Santillan, "Short-term forecasting models for photovoltaic plants: analytical versus soft-computing techniques," *Mathematical Problems in Engineering*, vol. 2013, Article ID 767284, 9 pages, 2013.

[27] S. Krinidis and V. Chatzis, "A robust fuzzy local information C-means clustering algorithm," *IEEE Transactions on Image Processing*, vol. 19, no. 5, pp. 1328–1337, 2010.

[28] W. Cui, Y. Wang, T. Lei, Y. Fan, and Y. Feng, "Brain MR image segmentation based on an adaptive combination of global and local fuzzy energy," *Mathematical Problems in Engineering*, vol. 2013, Article ID 316546, 10 pages, 2013.

[29] K.-K. Shyu, V.-T. Pham, T.-T. Tran, and P.-L. Lee, "Global and local fuzzy energy-based active contours for image segmentation," *Nonlinear Dynamics*, vol. 67, no. 2, pp. 1559–1578, 2012.

[30] O. C. Yolcu, "A hybrid fuzzy time series approach based on fuzzy clustering and artificial neural network with single multiplicative neuron model," *Mathematical Problems in Engineering*, vol. 2013, Article ID 560472, 9 pages, 2013.

[31] C. L. Pereira, C. A. C. M. Bastos, T. I. Ren, and G. D. C. Cavalcanti, "Fuzzy active contour models," in *Proceedings of the IEEE International Conference on Fuzzy Systems (FUZZ '11)*, pp. 1621–1627, Taipei, Taiwan, June 2011.

[32] X. Niu, G. Wang, W. Liang, H. Hou, H. Wang, and J. Zhang, "Application of fuzzy set theory to quantitative analysis of correctness of the mathematical model based on the ADI method during solidification," *Mathematical Problems in Engineering*, vol. 2013, Article ID 894384, 7 pages, 2013.

[33] C. Hwang and F. C.-H. Rhee, "Uncertain fuzzy clustering: interval type-2 fuzzy approach to C-means," *IEEE Transactions on Fuzzy Systems*, vol. 15, no. 1, pp. 107–120, 2007.

[34] N. N. Karnik and J. M. Mendel, "Applications of type-2 fuzzy logic systems to forecasting of time-series," *Information Sciences*, vol. 120, no. 1, pp. 89–111, 1999.

[35] Q. Liang and J. M. Mendel, "Equalization of nonlinear time-varying channels using type-2 fuzzy adaptive filters," *IEEE Transactions on Fuzzy Systems*, vol. 8, no. 5, pp. 551–563, 2000.

[36] H. A. Hagras, "A hierarchical type-2 fuzzy logic control architecture for autonomous mobile robots," *IEEE Transactions on Fuzzy Systems*, vol. 12, no. 4, pp. 524–539, 2004.

[37] Q. Liang and J. M. Mendel, "MPEG VBR video traffic modeling and classification using fuzzy technique," *IEEE Transactions on Fuzzy Systems*, vol. 9, no. 1, pp. 183–193, 2001.

[38] C.-A. Deledalle, L. Denis, and F. Tupin, "Iterative weighted maximum likelihood denoising with probabilistic patch-based weights," *IEEE Transactions on Image Processing*, vol. 18, no. 12, pp. 2661–2672, 2009.

[39] H. L. Wan and L. C. Jiao, "Change detection in SAR images by means of grouping connected regions using clone selection algorithm," *Electronics Letters*, vol. 47, no. 5, pp. 338–339, 2011.

[40] T. Celik, "Image change detection using Gaussian mixture model and genetic algorithm," *Journal of Visual Communication and Image Representation*, vol. 21, no. 8, pp. 965–974, 2010.

[41] D.-D. Yang, L.-C. Jiao, M.-G. Gong, and F. Liu, "Artificial immune multi-objective SAR image segmentation with fused complementary features," *Information Sciences*, vol. 181, no. 13, pp. 2797–2812, 2011.

[42] A. Raychaudhuri, S. Khandelwal, S. Chhalani, and N. Kakarania, "Change detection in remote sensing images using elitist genetic algorithm," *International Journal of Emerging Technology and Advanced Engineering*, vol. 2, no. 7, pp. 2250–2459, 2012.

[43] J. Mendel, *Uncertain Rule-Based Fuzzy Logic Systems: Introduction and New Directions*, Prentice Hall, 2001.

[44] T. Celik, "Change detection in satellite images using a genetic algorithm approach," *IEEE Geoscience and Remote Sensing Letters*, vol. 7, no. 2, pp. 386–390, 2010.

[45] N. Otsu, "A threshold selection method from gray-level histograms," *IEEE Transactions on Systems, Man and Cybernetics*, vol. 9, no. 1, pp. 62–66, 1979.

[46] P. L. Rosin and E. Ioannidis, "Evaluation of global image thresholding for change detection," *Pattern Recognition Letters*, vol. 24, no. 14, pp. 2345–2356, 2003.

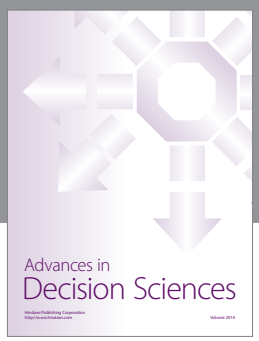

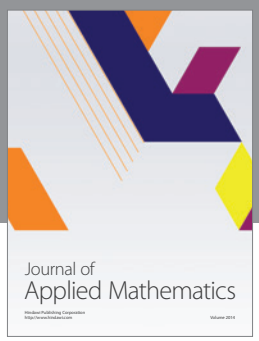

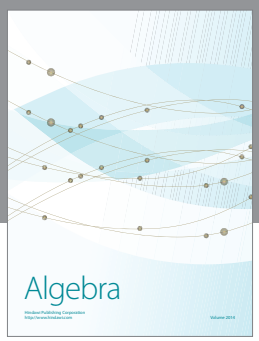

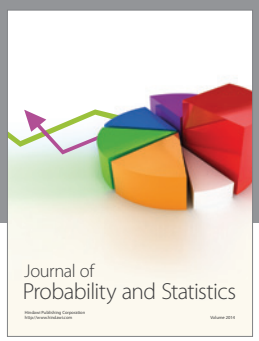

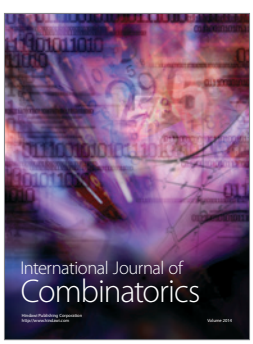

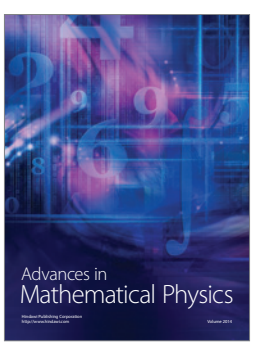

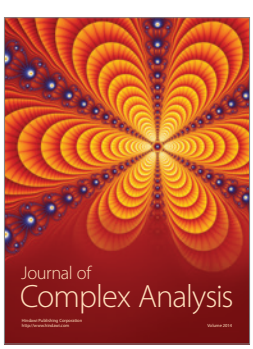

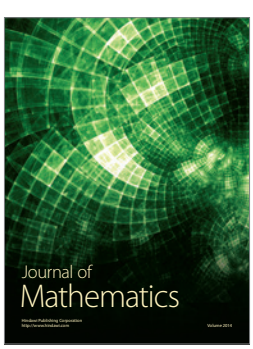

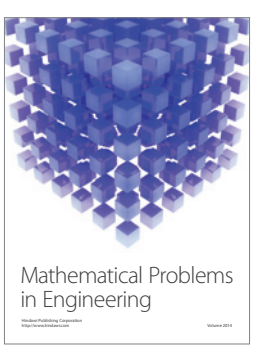

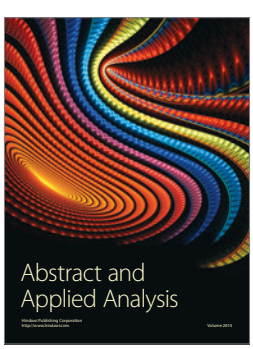

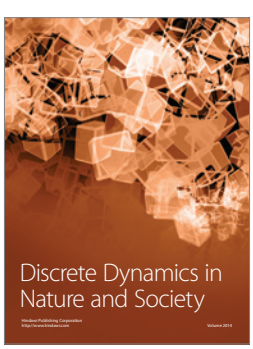

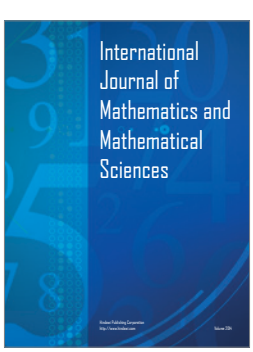

Hindawi

Submit your manuscripts at
http://www.hindawi.com